

Multimodal hierarchical Variational AutoEncoders with Factor Analysis latent space

Alejandro Guerrero-López^{a,b,*}, Carlos Sevilla-Salcedo^c, Vanessa Gómez-Verdejo^a, Pablo M. Olmos^{a,b}

^a*Department of Signal Processing and Communications, Universidad Carlos III de Madrid, Leganés, 28911, Spain*

^b*Instituto de Investigación Sanitaria Gregorio Marañón, Madrid, 28007, Spain*

^c*Department of Computer Science, Aalto University, Espoo, 02150, Finland*

Abstract

Real-world databases are complex and usually require dealing with heterogeneous and mixed data types making the exploitation of shared information between views a critical issue. For this purpose, recent studies based on deep generative models merge all views into a nonlinear complex latent space, which can share information among views. However, this solution limits the model's interpretability, flexibility, and modularity. We propose a novel method to overcome these limitations by combining multiple Variational AutoEncoders (VAE) with a Factor Analysis latent space (FA-VAE). We use VAEs to learn a private representation of each heterogeneous view in a continuous latent space. Then, we share the information between views by a low-dimensional latent space using a linear projection matrix. This way, we create a flexible and modular hierarchical dependency between private and shared information in which new views can be incorporated afterwards. Beyond that, we can condition pre-trained models, cross-generate data from different domains, and perform transfer learning between generative models.

Keywords: Multimodal, Heterogeneous, Flexible, Factor Analysis, VAE, Hierarchical

2010 MSC: 00-01, 99-00

1. Introduction

Many real-world problems require dealing with heterogeneous and mixed data types. For instance, combining cloud images and multimodal information, such as temperature, humidity, pressure, and wind speed, enhances cloud classification [1]. Similarly, fusion multimodal sensor streams, such as cameras, lidar, radar measurements, and environmental sensors, e.g., temperature, wind

*Corresponding author

Email address: alexjorguer@tsc.uc3m.es (Alejandro Guerrero-López)

speed, and humidity, improve object detection for autonomous vehicles [2]. Even in microbiology, the combination of spectrograms, epidemiological data, and antibiotic resistance optimizes the automatic discrimination of bacteria [3, 4].

Deep generative models emerge as a powerful methodology to learn from these multimodal data, since they have demonstrated their ability to create diverse and realistic synthetic data such as images [5, 6, 7], text [8, 9, 10], or audio signals [11, 12, 13]. Deep hierarchical VAEs [14, 15, 16, 17] further divide the latent space into disjoint groups of latent variables to increase the expressiveness of both the approximate posterior and prior distributions. They are robust models capable of disentangling private and shared information into hierarchical latent variables [18, 19, 20, 21]. However, training deep hierarchical models creates inference bias due to approximate inference techniques, requiring time-costly techniques such as Hamiltonian Monte Carlo sampling [22, 20].

Learning from multimodal data does not only require exploring complex latent spaces with hierarchical relations but also requires novel design methodologies to incorporate the different data modalities or views in a structured manner. This structure has been widely studied in recent years. In JMVAE [23], the authors project two different views on a shared latent space using a bidirectional double VAE. Meanwhile, in JVA²E [24], they combine adversarial learning with the generative VAE's latent features. Other works, such as MVAE [25], combine K input views using an individual encoder per view; then, it creates a common latent space representation by a Gaussian Product-of-Experts (PoE) given the private representations, following the same structure as in DMVAE [26]. In MMVAE [27], the authors propose a generalization of MVAE and DMVAE by substituting the PoE with a Mixture of Experts obtaining more realistic cross-generated data. Following a similar idea, in AMVAE [28], the K views are projected into a common latent space using a fully-connected layer. In Multi-VAE [29], the authors propose a probabilistic change where a private continuous latent variable represents each view and categorical discrete latent variable models the shared information. These and other concurrent approaches to handling multi-view data share a common aspect. They all rely on a complex hierarchical deep latent representation to project the data correlation among views. This complexity brings a lack of modularity to add new data views when available and to handle missing views; it also hinders inference training and obscures the interpretability of the model in terms of the dependency of the latent spaces with the different views.

In this paper, we demonstrate how a two-level hierarchy composed of local per-view VAE-like models combined with a linear factor-analysis (FA) global latent space, FA-VAE, is flexible and robust enough to effectively handle multi-view data problems with significant advantages w.r.t. the models mentioned above. FA-VAE is iteratively trained in two steps. First, it updates independently every per-view local VAE model modifying their prior distribution. Then, the global FA model is updated by a closed-form mean-field formulation. These updates further allow a modular approach in which pre-training can be carried out and incorporate new views afterward. Beyond that, these updates handle missing views naturally. Finally, we proposed Automatic Relevance Determination (ARD) priors on the

FA weight matrices, allowing us to analyze the importance of every global latent dimension to explain each data view, allowing for better interpretability.

We demonstrate the features of the FA-VAE model with different representative experimental setups. Firstly, we borrow a pre-trained unsupervised VAE and use FA-VAE to condition it to a set of given attributes with a few mean-field updates. Secondly, we perform domain adaptation between different image datasets by combining multiple VAEs, which can be individually pre-trained. Furthermore, finally, we demonstrate how FA-VAE can be used to speed up the training of deep complex VAEs by doing transfer learning from a small, simple VAE model over the same dataset. We believe that none of the papers in the state-of-the-art can provide such a level of flexibility, complexity, and modularity. The code to reproduce every experiment is available at github.com/aguerrero/FA-VAE.

The article is organized as follows: Section 2 reviews the Sparse Semi-supervised Heterogeneous Interbattery Bayesian Analysis (SSHIBA) [30] and the VAE [31] formulations and, introduces the proposed formulation of FA-VAE. Section 3 defines three experiments to demonstrate that the proposed approach: (i) can condition a pre-trained VAE, (ii) performs domain adaptation, and (iii) can transfer learning between VAEs. Finally, Section 4 gives some final remarks and highlights the main results.

2. Methods

2.1. Sparse Semi-supervised Heterogeneous Interbattery Bayesian Analysis

SSHIBA [30, 32] presents a solution to multi-view problems with samples represented in M different modalities where each view can be either multilabel, binary, real, categorical, or other multidimensional objects. The general model framework, depicted in Fig. 1a, considers that the n -th sample of the m -th view, $\mathbf{x}_{n,:}^{(m)} \in \mathbb{R}^{1 \times D}$, can be projected into a low-dimensional latent space, $\mathbf{g}_{n,:} \in \mathbb{R}^{1 \times K_c}$ where K_c is the number of latent factors of this common space. As seen in Fig. 1b, the m -th view for the n -th observation, $\mathbf{x}_{n,:}^{(m)}$, can be generated by linearly combining $\mathbf{g}_{n,:}$ with a projection matrix $\mathbf{W}^{(m)} \in \mathbb{R}^{D \times K_c}$, i.e.,

$$\mathbf{x}_{n,:}^{(m)} = \mathbf{g}_{n,:} \mathbf{W}^{(m)\top} + \tau^{(m)}, \quad (1)$$

where $\tau^{(m)}$ is zero-mean Gaussian noise, with noise power following a Gamma distribution of parameters $a^{\tau^{(m)}}$ and $b^{\tau^{(m)}}$. SSHIBA also includes a column-wise ARD prior [33] over each view’s projection matrix through the variable $\alpha_k^{(m)}$ which follows a Gamma distribution, $\alpha_k^{(m)} \sim \Gamma(a^{\alpha^{(m)}}, b^{\alpha^{(m)}})$. This prior removes the need for cross-validating the number of latent factors. It implies that each $\mathbf{W}^{(m)}$ effectively selects which part of the global latent space \mathbf{G} is specific to each m -view (intra-view) or shared among views (inter-view).

The model is trained by evaluating the posterior distribution of all rv given the observed data. However, due to the intractability of these posteriors, they are

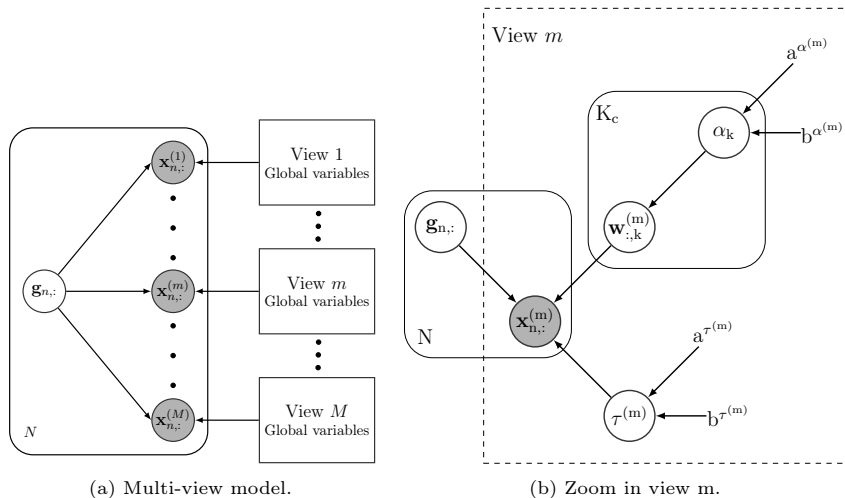


Figure 1: SSHIBA basic structure. Gray circles denote observations, white circles represent random variables (rv), and the non-circles are hyper-parameters. Subfigure 1a represents the latent space projection $\mathbf{g}_{n,:}$ given all m input views and subfigure 1b represents how a real m -view is modeled.

approximated through mean-field Variational Inference (VI) [34] to the posterior distribution with a fully factorized variational family q as:

$$p(\Theta|\mathbf{X}^{(m)}) \approx \prod_{m=1}^M (q(\mathbf{W}^{(m)})q(\tau^{(m)}) \prod_{k=1}^{K_c} q(\alpha_k^{(m)})) \prod_{n=1}^N q(\mathbf{g}_{n,:}), \quad (2)$$

where Θ is a vector of all rv in the model, shown in Fig. 1b. Therefore, combining the mean-field posterior with the Evidence LowerBound (ELBO) results in a feasible coordinate-ascent-like optimization algorithm where each rv is computed by maintaining the rest fixed following:

$$q^*(\mathbf{G}) \propto \mathbb{E}_{\Theta_{-i}}[\log p(\Theta_{-i}, \mathbf{g}_{1,:}, \dots, \mathbf{g}_{N,:})] \quad (3)$$

with Θ_{-i} being all rv but θ_i . Using this formulation, we create an efficient and feasible optimization problem since it does not require a complete marginalization of all Θ rv from the joint distribution. The rules to update of every rv can be seen in Table 1. The complexity bottleneck of SSHIBA is to invert $\Sigma_{\mathbf{G}}^{-1} \in \mathbb{R}_+^{K_c \times K_c}$, and to invert $\Sigma_{\mathbf{W}^{(m)}}^{-1} \in \mathbb{R}_+^{D \times D}$, where for high-dimensional data kernel methods can be used as demonstrated in [32].

Furthermore, the Bayesian nature of the model allows it to work in a semi-supervised fashion, using all available information to determine the approximate distribution of the variables. In turn, the model can marginalize any missing values in the data and predict test samples for any view by sampling from its variational distribution.

Table 1: Updated distributions for the different rv of the model. These expressions have been obtained using the update rules of the mean field approximation. See [30] for further details.

Variable	q^* distribution	Parameters
$\mathbf{g}_{n,:}$	$\mathcal{N}(\mathbf{g}_{n,:} \mu_{\mathbf{g}_{n,:}}, \Sigma_{\mathbf{G}})$	$\mu_{\mathbf{g}_{n,:}} = \sum_{m=1}^M \left(\langle \tau^{(m)} \rangle \mathbf{X}^{(m)} \langle \mathbf{W}^{(m)} \rangle \Sigma_{\mathbf{G}} \right)$ $\Sigma_{\mathbf{G}}^{-1} = \mathbf{I}_{K_c} + \sum_{m=1}^M \left(\langle \tau^{(m)} \rangle \langle \mathbf{W}^{(m)T} \mathbf{W}^{(m)} \rangle \right)$
$\mathbf{W}^{(m)}$	$\prod_{d=1}^{D_m} \mathcal{N}(\mathbf{w}_{d,:}^{(m)} \mu_{\mathbf{w}_{d,:}^{(m)}}, \Sigma_{\mathbf{W}^{(m)}})$	$\mu_{\mathbf{w}_{d,:}^{(m)}} = \langle \tau^{(m)} \rangle \mathbf{X}^{(m)T} \langle \mathbf{G} \rangle \Sigma_{\mathbf{W}^{(m)}}$ $\Sigma_{\mathbf{W}^{(m)}}^{-1} = \text{diag}(\langle \boldsymbol{\alpha}^{(m)} \rangle) \langle \gamma_d^{(m)} \rangle + \langle \tau^{(m)} \rangle \langle \mathbf{G}^T \mathbf{G} \rangle$
$\boldsymbol{\alpha}^{(m)}$	$\prod_{k=1}^{K_c} \Gamma(\alpha_k^{(m)} a_{\alpha_k^{(m)}}, b_{\alpha_k^{(m)}})$	$a_{\alpha_k^{(m)}} = \frac{D_m}{2} + a^{\boldsymbol{\alpha}^{(m)}}$ $b_{\alpha_k^{(m)}} = b^{\boldsymbol{\alpha}^{(m)}} + \frac{1}{2} \sum_{d=1}^{D_m} \langle \gamma_d^{(m)} \rangle \langle \mathbf{w}_{d,k}^{(m)} \mathbf{w}_{d,k}^{(m)} \rangle$
$\tau^{(m)}$	$\Gamma(\tau^{(m)} a_{\tau^{(m)}}, b_{\tau^{(m)}})$	$a_{\tau^{(m)}} = \frac{D_m N}{2} + a^{\tau^{(m)}}$ $b_{\tau^{(m)}} = b^{\tau^{(m)}} + \frac{1}{2} \left(\sum_{n=1}^N \sum_{d=1}^{D_m} x_{n,d}^{(m)2} - 2 \text{Tr}(\langle \mathbf{W}^{(m)} \rangle \langle \mathbf{G}^T \rangle \mathbf{X}^{(m)}) + \text{Tr}(\langle \mathbf{W}^{(m)T} \mathbf{W}^{(m)} \rangle \langle \mathbf{G}^T \mathbf{G} \rangle) \right)$

2.2. Variational AutoEncoders

A Variational AutoEncoder (VAE) is a probabilistic model that assumes there exists a hidden latent variable $\mathbf{z} \in \mathbb{R}^{1 \times D'}$ capable of generating the observations $\mathbf{x} \in \mathbb{R}^{1 \times D}$ through a non-linear model. D represents the observation dimension and D' is a hyper-parameter. The latent variables are inferred from the observations following:

$$p_{\theta}(\mathbf{z}|\mathbf{x}) = \frac{p_{\theta}(\mathbf{x}|\mathbf{z})p(\mathbf{z})}{p(\mathbf{x})}, \quad (4)$$

where, $p_{\theta}(\mathbf{x}|\mathbf{z})$ corresponds to the decoder, which is based on a Neural Network (NN) parametric model with θ parameters, and $p_{\theta}(\mathbf{z}|\mathbf{x})$ is the encoder (see in Fig. 2 the probabilistic model). However, its computation by means of Eq. (4) is not feasible, since computing $p(\mathbf{x})$ is intractable. Hence, we use VI to approximate it with a tractable parameterized family of distributions defined as $q_{\eta}(\mathbf{z}|\mathbf{x})$. To do so, we minimize KL divergence between the two distributions:

$$\min_{\eta} \text{KL}(q_{\eta}(\mathbf{z}|\mathbf{x}) || p_{\theta}(\mathbf{z}|\mathbf{x})) \quad (5)$$

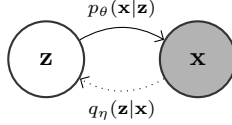


Figure 2: VAE basic structure, where $q_\eta(\mathbf{z}|\mathbf{x})$ is the encoder network and $p_\theta(\mathbf{x}|\mathbf{z})$ is the decoder network. Gray circles denote observations, and white circles represent rv.

which is equivalent to maximizing the following ELBO [31]:

$$\mathcal{L}_{\theta,\eta} = \underbrace{\mathbb{E}_{q_\eta(\mathbf{z}|\mathbf{x})}[\log(p_\theta(\mathbf{x}|\mathbf{z}))]}_{\mathbf{I}} - \underbrace{\text{KL}(q_\eta(\mathbf{z}|\mathbf{x})||p(\mathbf{z}))}_{\mathbf{II}}, \quad (6)$$

where the likelihood term **I** drives the reconstruction of the observations and **II** ensures that the learned distribution $q_\eta(\mathbf{z}|\mathbf{x})$ is similar to the prior distribution $p(\mathbf{z})$.

Here, we use a variant of this model called β -VAE [35] which multiplies the regularization term by a β hyper-parameter ($\beta > 1$), resulting in a more disentangled latent representation when the prior $p(\mathbf{z})$ is independent.

2.3. Factor Analysis Variational AutoEncoder

We propose a novel hierarchical method, Factor Analysis VAE (FA-VAE), that combines multiple VAEs by disentangling the private and shared information of heterogeneous observations via SSHIBA. In particular, our proposal uses the multiview nature of SSHIBA to join the latent information from different VAEs in a shared latent space. Given the m -view, we represent its private information by a continuous latent variable, $\mathbf{z}_{n,:}^{(m)}$, provided by a VAE. Then, all private latent variables $\mathbf{z}_{n,:}^{(m)}$, for $m = 1, \dots, M$, project their shared information into a global latent variable, $\mathbf{g}_{n,:}$.

To calculate the private latent representation of the m -th view, we use a VAE that encodes the observations using the variational distribution $\mathbf{z}_{n,:}^{(m)} | \mathbf{x}_{n,:}^{(m)} \sim q_\eta(\mathbf{z}_{n,:}^{(m)})$, defined as

$$q_\eta(\mathbf{z}_{n,:}^{(m)}) \sim \mathcal{N}\left(\mu_\eta^{\mathbf{z}^{(m)}}(\mathbf{x}_{n,:}^{(m)}), \Sigma_\eta^{\mathbf{z}^{(m)}}(\mathbf{x}_{n,:}^{(m)})\right), \quad (7)$$

where $\mu_\eta^{\mathbf{z}^{(m)}}(\mathbf{x}_{n,:}^{(m)})$, $\Sigma_\eta^{\mathbf{z}^{(m)}}(\mathbf{x}_{n,:}^{(m)})$ are the output of an independent parametric encoder for the m -th view. Fig. 3 shows the FA-VAE's graphical model where the generative model assumes that

$$\mathbf{z}_{n,:}^{(m)} \sim \mathcal{N}\left(\mathbf{g}_{n,:} \mathbf{W}^{(m)}, \tau^{(m)-1}\right), \quad (8)$$

and, thus, the observations $\mathbf{x}_{n,:}^{(m)}$ are generated from $\mathbf{z}_{n,:}^{(m)}$ (8) using the VAE

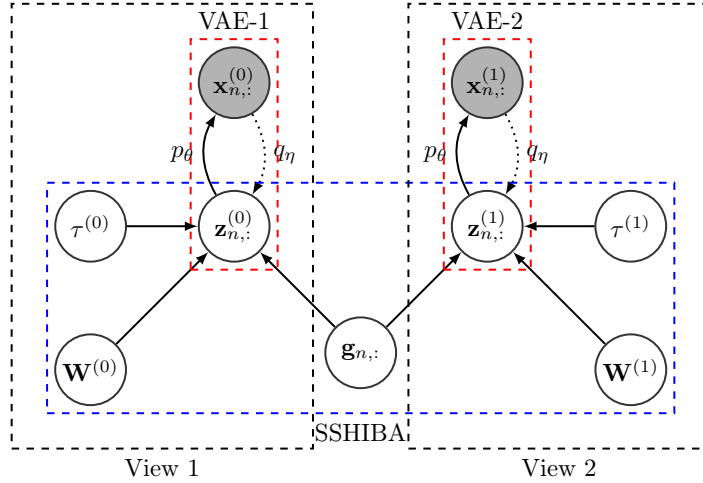


Figure 3: FA-VAE graphical model example with two VAEs. The blue dotted rectangle denotes the SSHIBA rv while the red rectangles indicate the two VAEs structures, one per view. Gray circles denote observations, and white circles represent rv.

conditional distribution $\mathbf{x}_{n,:}^{(m)} | \mathbf{z}_{n,:}^{(m)} \sim p_{\theta}(\mathbf{x}_{n,:}^{(m)} | \mathbf{z}_{n,:}^{(m)})$, which we define as

$$\mathbf{x}_{n,:}^{(m)} \sim \mathcal{N}\left(\mu_{\theta}^{\mathbf{x}_{n,:}^{(m)}}(\mathbf{z}_{n,:}^{(m)}), \sigma\right) \quad (9)$$

where $\mu_{\theta}^{\mathbf{x}_{n,:}^{(m)}}(\mathbf{z}_{n,:}^{(m)})$ is the output of an independent parametric decoder for the m -th view with σ fixed.

Regarding each m -th pair encoder-decoder, we can arbitrarily choose their internal structure. This flexibility allows FA-VAE to model heterogeneous observations, in addition to those that SSHIBA could already model, such as images with a Convolutional Neural Network (CNN) or sequential data with a Recursive Neural Network (RNN).

As shown in Eq. (6), the ELBO maximization of a VAE ensures that the variational distribution $q_{\eta}(\mathbf{z}_{n,:}^{(m)} | \mathbf{x}_{n,:}^{(m)})$ is close to the prior distribution $p(\mathbf{z})$ by minimizing their KL divergence. Standard VAE formulation usually considers that $p(\mathbf{z}) \sim \mathcal{N}(0, I)$, however, in SSHIBA's framework the prior over $\mathbf{z}_{n,:}^{(m)}$ is imposed by Factor Analysis (FA) decomposition. Thus, to integrate both models, we have to obey Eq. (8), where $\mathbf{g}_{n,:}$, $\mathbf{W}^{(m)}$, and $\tau^{(m)}$ are sampled from their posterior distribution (see Table 1). Therefore, the ELBO maximized by each m -VAE is

$$\begin{aligned} \mathcal{L}^{(m)} = & \mathbb{E}_{q_{\eta}(\mathbf{z}_{n,:}^{(m)} | \mathbf{x}_{n,:}^{(m)})} \log \left(p_{\theta}(\mathbf{x}_{n,:}^{(m)} | \mathbf{z}_{n,:}^{(m)}) \right) \\ & - \beta \text{KL} \left(q_{\eta}(\mathbf{z}_{n,:}^{(m)} | \mathbf{x}_{n,:}^{(m)}) || \mathcal{N} \left(\mathbf{g}_{n,:}, \mathbf{W}^{(m)}, \tau^{(m)-1} \right) \right), \end{aligned} \quad (10)$$

where the first term is the Gaussian Log-Likelihood (GLL) between $\mathbf{x}_{n,:}^{(m)}$ and samples from $p_\theta(\mathbf{x}_{n,:}^{(m)} | \mathbf{z}_{n,:}^{(m)})$, and the second term minimizes the KL divergence between the variational distribution and SSHIBA’s rv.

Finally, using the mean-field approach, we calculate each $q(\theta_i)$ following Table 1 where, in case of updating a m -VAE views, $\mathbf{X}^{(m)}$ is now sampled by the encoder $q(\mathbf{Z}^{(m)})$ resulting in $\mathbf{Z}^{(m)}$ samples. Following this procedure, FA-VAE trains according to the steps detailed in Algorithm 1.

Algorithm 1: FA-VAE training algorithm

```

Initialise  $\mathbf{G}, \mathbf{W}^{(m)}, \mathbf{z}_{n,:}^{(m)}, \alpha_k^{(m)}, \tau^{(m)}$ ;
while FA-VAE not converge do
    Update  $q(\mathbf{G})$  following 1st row of Table 1;
    for each  $m$ -view do
        Update  $q(\mathbf{W}^{(m)})$  following 2nd row of Table 1;
        for each epoch do
            | Maximise the  $m$ -VAE’s ELBO (Eq. (10)) ;
        end
        Update  $q(\mathbf{z}_{n,:}^{(m)})$  sampling from  $q_\eta(\mathbf{z}_{n,:}^{(m)}) \sim \mathcal{N}(\mu_\eta^{\mathbf{z}_{n,:}^{(m)}}, \Sigma_\eta^{\mathbf{z}_{n,:}^{(m)}})$ ;
        Update  $q(\alpha_k^{(m)})$  following 3th row of Table 1;
        Update  $q(\tau^{(m)})$  following 4th row of Table 1;
    end
end

```

3. Experiments

Throughout this section, we demonstrate the flexibility of FA-VAE in addressing relevant problems in deep probabilistic modeling. In Section 3.1, we analyze how FA-VAE can condition a pre-trained VAE to multilabel targets. In Section 3.2, we apply it over a domain adaptation problem and compare it to the Multi-VAE model [29]. Besides, we disentangle and analyze the private-shared latent variables. Finally, in Section 3.3 we use the proposed FA-VAE’s framework to perform transfer learning between multiple VAEs, showing how the transfer learning creates a more expressive and understandable latent space than other models such as β -VAE [35]. The code to reproduce the following experiments can be found at github.com/aguerrero/FA-VAE.

3.1. FA-VAE as a conditioned generative model

In this scenario, we show how we can use FA-VAE’s framework to easily adapt a pre-trained unconditioned VAE, $p_\theta(\mathbf{x})$, to model a conditional distribution, $p_\theta(\mathbf{x}|\mathbf{a})$, for a given set of labeled data $\{\mathbf{x}_i, \mathbf{a}_i\}_{i=1}^N$ where \mathbf{x}_i is an observation and \mathbf{a}_i is an attribute. For this experiment, we use CelebA dataset [36] restricted to 30000 samples, and we select three attributes: wearing lipstick, gender, and

smiling. Therefore, we use $30000 \times 64 \times 64 \times 3$ RGB images with a stratified proportion of these three attributes.

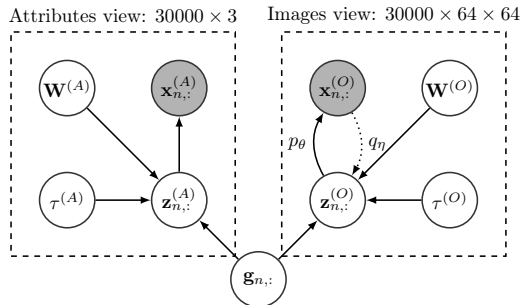


Figure 4: Conditioning a single VAE to a multilabel attribute vector using FA-VAE architecture where A denotes attributes view and O observations views. Gray circles are observations, and white circles represent rv.

Using the FA-VAE multi-view framework, we propose to model the problem with a two-view setup following the graphical model shown in Fig. 4. The first view is in charge of modeling the attributes (A) as a multilabel vector with three attributes: wearing lipstick, female/male, and smiling. For this view, we use the standard multilabel SSHIBA’s configuration without any VAE. In this case, we generate the binary attributes, denoted as $\mathbf{x}_{n,:}^{(A)}$, from the private variable $\mathbf{z}_{n,:}^{(A)}$ using a Bernoulli distribution as

$$p(\mathbf{x}_{n,:}^{(A)} | \mathbf{z}_{n,:}^{(A)}) = \prod_{d=1}^3 e^{z_{n,d}^{(A)} x_{n,d}^{(A)}} \sigma\left(-z_{n,d}^{(A)}\right) \quad (11)$$

where σ is the sigmoidal function.

The second view (O) is composed by observed RGB images, denoted as $\mathbf{x}_{n,:}^{(O)} \in \mathbb{R}^{64 \times 64 \times 3}$. For both encoder and decoder, we borrow the network structure proposed in the β -VAE paper [37]. Namely, we use a CNN network with 5 convolutional layers of 64, 128, 256, 512, 1024 channel size with kernel size of 4, stride of 2, and padding 1. This CNN structure is followed by a fully connected layer to generate μ_η , and Σ_η and, then, infer the real pseudo-observation $\mathbf{z}_{n,:}^O \in \mathbb{R}^{100}$. The decoder follows the inverse structure of the encoder.

We train from scratch an unconditioned vanilla VAE over CelebA until convergence. Then, we add this unconditioned pre-trained vanilla VAE inside FA-VAE’s architecture to condition it to the attributes. Fig 5 analyses the model convergence for these two steps. In particular, Fig. 5a analyses the ELBO of the vanilla VAE trained from scratch, whereas Fig. 5b shows the ELBO evolution during the FA-VAE’s fine-tuning. This curve indicates that the pre-trained VAE keeps stable and does not lose reconstruction power. Therefore, we can condition a pre-trained VAE without interfering with its learning.

We can use this model to alter the attributes of a given image. To illustrate it,

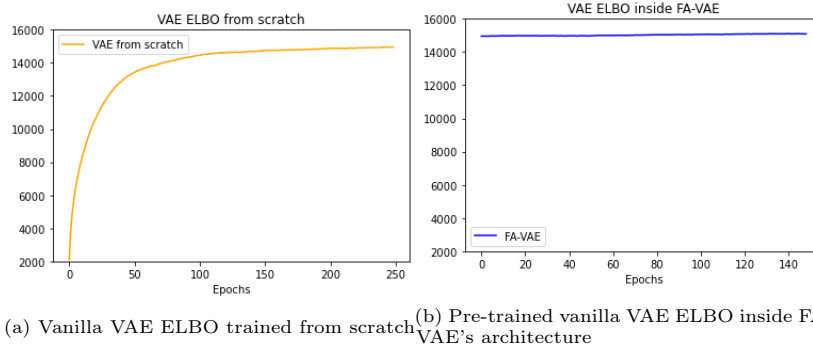


Figure 5: VAEs convergence by its own and inside FA-VAE’s architecture. Fig. 5a shows the ELBO of a vanilla VAE trained over CelebA from scratch. In Fig. 5b we plug the vanilla VAE from Fig. 5a inside FA-VAE’s architecture.

we project a CelebA image $\mathbf{x}_{n,:}^{(O)}$ to its private latent space $\mathbf{z}_{n,:}^{(O)}$ using $q_{\eta}(\mathbf{z}_{n,:}^{(O)} | \mathbf{x}_{n,:}^{(O)})$ and fix $\mathbf{z}_{n,:}^{(O)}$ as our reference image. Then, we select a set of attributes to change our image, and we generate $\mathbf{z}_{n,:}^{(A)}$. Then, using the posterior distribution of $\mathbf{g}_{n,:}$ (see Table 1):

$$\begin{aligned} \Sigma_{\mathbf{g}_{n,:}}^{-1} &= \mathbf{I}_{K_c} + \left(\langle \tau^{(A)} \rangle \langle \mathbf{W}^{(A)\top} \mathbf{W}^{(A)} \rangle \right) + \left(\langle \tau^{(O)} \rangle \langle \mathbf{W}^{(O)\top} \mathbf{W}^{(O)} \rangle \right) \\ \mu_{\mathbf{g}_{n,:}} &= \left(\langle \tau^{(A)} \rangle \mathbf{z}_{n,:}^{(A)} \langle \mathbf{W}^{(A)} \rangle \Sigma_{\mathbf{g}_{n,:}}^* + \langle \tau^{(O)} \rangle \mathbf{z}_{n,:}^{(O)} \langle \mathbf{W}^{(O)} \rangle \Sigma_{\mathbf{g}_{n,:}}^* \right) \end{aligned} \quad (12)$$

We can generate samples from the shared view, $\mathbf{g}_{n,:}^*$, for the fixed $\mathbf{z}_{n,:}^{(O)}$ and the private representations of the given attributes $\mathbf{z}_{n,:}^{(A)}$. Afterwards, we sample $\mathbf{z}_{n,:}^{*(O)} \sim \mathcal{N}(\mathbf{g}_{n,:}^*, \mathbf{W}^{(O)}, \tau^{(O)})$ and generate images using FA-VAE’s generative distribution $p_{\theta}(\mathbf{x}_{n,:}^{*(O)} | \mathbf{z}_{n,:}^{*(O)})$. Figs. 6a and 6b show the images resulting of this process. As can be seen, we can change either the gender of the input image (right column), make the face smile (bottom row), or remove the smiling (top row). We can also generate random images conditioned to any arbitrary set of attributes, as can be seen in Appendix A.1.

3.2. Domain adaptation

Due to FA-VAE’s modularity, we can go one step further and combine multiple VAEs simultaneously. For this purpose, let’s consider an illustrative example based on CelebA [36] dataset and Google Cartoon Set [38] dataset and, let’s consider a three view FA-VAE configuration (Fig. 7). We train a VAE with 10000 CelebA images on the first view. Then, we train another VAE with 10000 Cartoon set images on the second view. Moreover, in the third view, we add a binary label to model the hair color with a SSHIBA layer.

We hypothesize that the private latent variables $\mathbf{z}_{n,:}^{(m)}$ can capture the domain information of face images, cartoon avatars, and hair color. Then, the shared

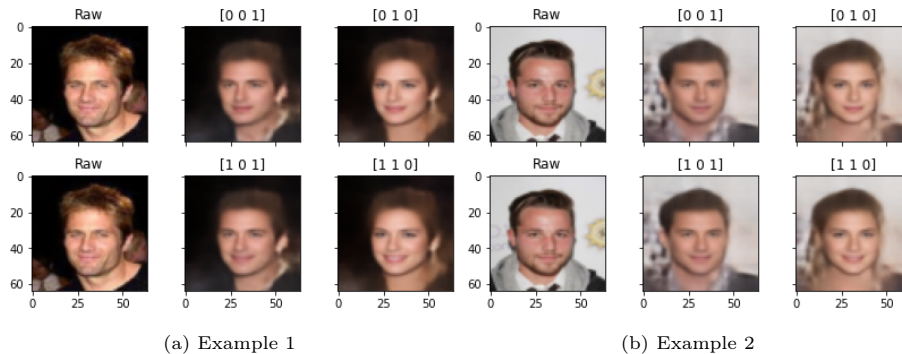


Figure 6: Different faces are generated by FA-VAE when modifying their attributes. The left column of each subfigure represents the raw image. Each subfigure’s center and right columns represent the altered images by changing the different attributes indicated in the title, meaning [smile, lipstick, gender].

latent space variable, $\mathbf{g}_{n,:}$, works as a bridge between domains to adapt real-world faces to 2D cartoon avatars given a hair color.

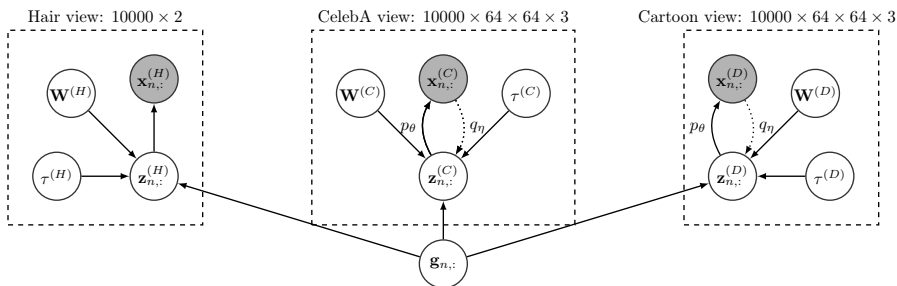


Figure 7: FA-VAE configuration to perform domain adaptation between two VAE-based views representing real-world faces (CelebA) and cartoon avatars (Cartoon) while conditioning to a third categorical view (hair). Gray circles denote observations, and white circles represent rv.

The CelebA view (C) is composed of $10000 \times 64 \times 64 \times 3$ observations of images of real celebrity faces, whereas the Cartoon view (D) is composed of $10000 \times 64 \times 64 \times 3$ observations of cartoon avatar images. For both views, we use the β -VAE in [35] encoder-decoder configuration already proposed in Section 3.1 using $\beta > 1$ as the authors recommend. Finally, the hair view, H , is composed of a 10000×2 binary label indicating hair color label: blond or brunet.

We compare FA-VAE with the Multi-VAE [29] model which uses a \mathbf{c}_n discrete latent variable to share the context of all views (see Fig. 8). For this model, we incorporate the hair label as an extra-dimension in $\mathbf{x}_{n,:}^{(C)}$ and $\mathbf{x}_{n,:}^{(D)}$.

Fig. 9 shows how FA-VAE (second row) and Multi-VAE (third row) translate images from the CelebA domain (first row) to the Cartoon domain. Although the only attribute seen by the models is the hair color, FA-VAE outperformed Multi-VAE by capturing other inherent features, such as the use of sunglasses.

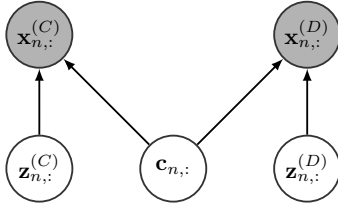


Figure 8: Conditioning two VAEs with a categorical variable using Multi-VAE model. CelebA images are represented by $\mathbf{x}_{n,:}^{(C)}$, Cartoon images are represented by $\mathbf{x}_{n,:}^{(D)}$, and the $\mathbf{c}_{n,:}$ captures the shared information. Gray circles denote observations, and white circles represent rv.

Moreover, Multi-VAE does not properly learn skin color, as seen in Images 3 and 9, while FA-VAE does. Finally, FA-VAE generates high-quality 2D avatars with no blur or artifacts.



Figure 9: Domain adaptation from CelebA dataset to Cartoon dataset. The first row represents the original observations in CelebA dataset. In contrast, the second and third rows represent their translation to the Cartoon domain using **FA-VAE** (second row) and **Multi-VAE** (third row).

The private latent variables $\mathbf{Z}^{(D)}$ and $\mathbf{Z}^{(C)}$ codify the information of each domain, while the global space \mathbf{G} enables information transference between both domains. We can use this to apply domain adaption by translating images from one domain to the other. For this purpose, first, we get two CelebA images and project them to their private latent space as $\mathbf{z}_{1,:}^{(C)}$ and $\mathbf{z}_{2,:}^{(C)}$. Then, we project them to the shared latent space $\mathbf{g}_{1,:}^{*}; \mathbf{g}_{2,:}^{*}$ to, later, sample from the cartoon private latent space $\mathbf{Z}^{(D)} \sim \mathcal{N}(\mathbf{g}_{n,:}^{*}; \mathbf{W}^{(D)}, \tau^{(D)})$, obtaining $\mathbf{z}_{1,:}^{(D)}$ and $\mathbf{z}_{2,:}^{(D)}$. Now, we interpolate the private representation of each pair of images in each domain using the convex combination

$$\mathbf{z}_{n,:}^{(m)}_{\lambda} = \lambda \mathbf{z}_{n,:}^{(m)}_{1} + (1 - \lambda) \mathbf{z}_{n,:}^{(m)}_{2}, \quad (13)$$

where $m \in [C, D]$ represents any of the two views, and $\lambda \in [0, 1]$ allows us to move from Image 1 to Image 2. Finally, using the generated private representation $\mathbf{z}_{\lambda}^{(m)}$ we can use $p_{\theta}^m(\mathbf{x}_{\lambda}^{(m)} | \mathbf{z}_{\lambda}^{(m)})$ to generate the sample of each domain. The

reconstructed sequences $\mathbf{x}_{\lambda,:}^{(m)} | \mathbf{z}_{\lambda,:}^{(m)}$ for different values of λ are shown in Fig. 10.



Figure 10: Examples of an image transformation and domain adaption application. The first and second rows show the evolution from $\mathbf{z}_{1,:}^{(C)}$ to $\mathbf{z}_{2,:}^{(C)}$ and, from $\mathbf{z}_{1,:}^{(D)}$ to $\mathbf{z}_{2,:}^{(D)}$, respectively.

In both rows of Fig. 10 we can see a complete evolution from one image to the other. Any point sampled from the latent space has generated a meaningful image, demonstrating completeness. Additionally, both images’ transitions are clean and gradual, demonstrating continuity. In the cartoon domain, we can see how the avatar evolves in hairstyle, hair color, and eyeglasses. Hence, both latent variables, $\mathbf{Z}^{(D)}$ and $\mathbf{Z}^{(C)}$, fulfill completeness and continuity; thus, both are informative and explainable. Similarly, the global latent space \mathbf{G} also demonstrates completeness and continuity, as shown in Appendix A.2.

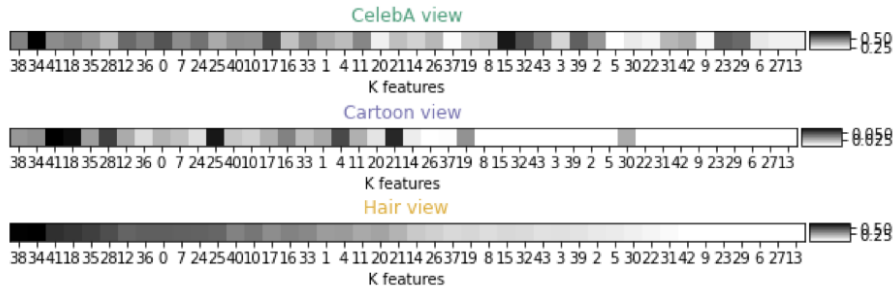


Figure 11: Mean over the rows of each $\mathbf{W}^{(m)}$ matrix. Each row is a vector representing the importance that each k latent feature of $\mathbf{g}_{n,:}$ has to reconstruct each view. The first row represents the CelebA view, the second row represents the Cartoon view, and the third row represents the Hair view.

Moreover, we can exploit the FA part of the model to analyze the relationship between all views visually. To do so, we compute the mean over the rows of each $\mathbf{W}^{(m)}$ matrix, thus, creating a row vector of length K . This vector represents the importance each K dimension of $\mathbf{g}_{n,:}$ has for each view. Fig. 11 includes the representation of the three $\mathbf{W}^{(m)}$. These representations are ordered by their weight value in the hair view. The first 22 and the 25th latent features of each $\mathbf{W}^{(m)}$ are shared between the three views meaning that 23 latent features are needed to explain the shared information between the three multimodal views. Similarly, latent feature 30 is shared exclusively between CelebA and Cartoon datasets, but it has no information about the hair. 5 latent factors are used exclusively by CelebA. Finally, we can see that almost all latent features are

needed to explain CelebA itself as it is the more complex dataset.

3.3. Transfer learning

The computational cost is one of the main challenges when training powerful VAEs. These profound variational and generative networks need to be trained for many epochs. Thus, we propose a novel method to speed up this process, using FA-VAE as a transfer learning tool between VAEs over the same domain.

Let us consider an illustrative example based on the CelebA dataset with a two-view set-up following the graphic model shown in Fig. 12. On the first view (V), we use a pre-trained vanilla VAE; in fact, we use the one trained in Section 3.1. As we plug a pre-trained VAE, we do not train both encoder and decoder; thus, $\mathbf{z}_{n,:}^{(V)}$ is going to be static. Then, on the second view (O), we start from the architecture of β -VAE shown in Section 3.1 and, to make it deeper, we add an extra final CNN layer of 2048 channel size with a kernel size of 4, a stride of 2, and padding 1 in the encoder. Correspondingly, the decoder presents the inversed structure.

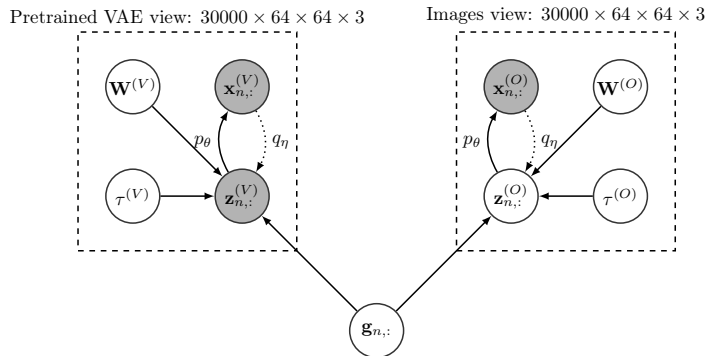


Figure 12: Transfer learning graphical model using FA-VAE. The V view represents information pre-learned by a vanilla VAE. As it is pre-trained, $\mathbf{z}_{n,:}^{(V)}$ is no longer a rv but an observation. The O view represents CelebA images using a β -VAE. Gray circles denote observations, and white circles represent rv.

We expect that the private space provided by a pre-trained vanilla VAE, $\mathbf{z}_{n,:}^{(V)}$, speeds up the training of a deeper VAE or even helps find a better global solution. To demonstrate this functionality, we compare two scenarios: our transfer learning approach using FA-VAE and a single β -VAE with the same structure as the second view of FA-VAE. Fig. 13 shows the performance of both approaches. As seen in Fig. 13a, FA-VAE presents an accurate reconstruction capability in the first epochs, meaning that the latent space of the vanilla VAE can provide a good initialization to β -VAE. Moreover, in terms of speed, FA-VAE gets the same maximum GLL as β -VAE in approximately four times fewer epochs. Furthermore, FA-VAE scores the highest absolute value in terms of GLL compared to β -VAE on its own. Looking at Fig. 13b, we can see that FA-VAE achieves a lower global KL term. The periodical spikes correspond to every time

the SSHIBA part of FA-VAE updates the VAE prior distribution as seen in Algorithm 1. Meanwhile, for β -VAE the KL starts increasing while FA-VAE directly goes down, justifying the better behavior since the beginning.

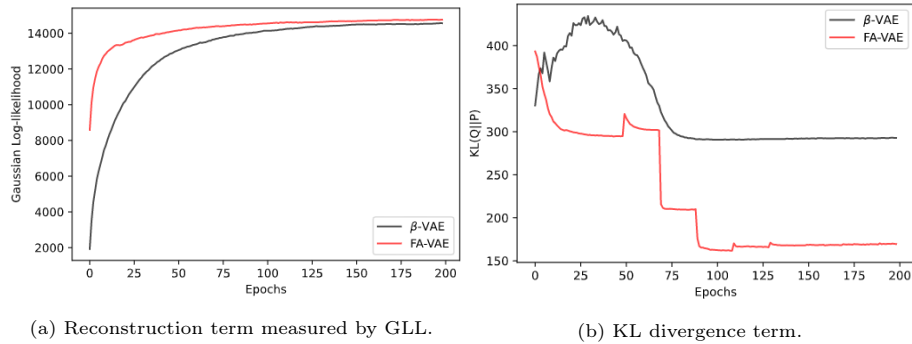


Figure 13: ELBO decomposition in reconstruction term and KL divergence term. The red line represents our approach, FA-VAE, while the black line represents the β -VAE on its own.

In Fig. 14, we show 5 random test images, i.e., never seen before by any of the models. We use β -VAE, FA-VAE, and Multi-VAE to encode the images to their private latent space and then reconstruct them back to their original domain. As it might not be apparent to the human eye which method reconstructs the images better, in Table 2, we include the R2 score on the reconstruction over 10000 test images. Here, we can see that FA-VAE provides better performance in terms of R2 score, demonstrating that transfer learning improves the model performance.

Another advantage of FA-VAE is its ability to create a more expressive and meaningful private latent representation of the images than β -VAE. To demonstrate this, we show the impact of arbitrarily modifying the 10 most relevant features. We select these based on the corresponding absolute values in the weight matrix $\mathbf{W}^{(m)}$, for both private latent variables: $\mathbf{z} \in \mathbb{R}^{1 \times 100}$ for β -VAE, and $\mathbf{z}_{n,:}^{(O)} \in \mathbb{R}^{1 \times 100}$. Then we randomly modify their values in the $[-20, 20]$

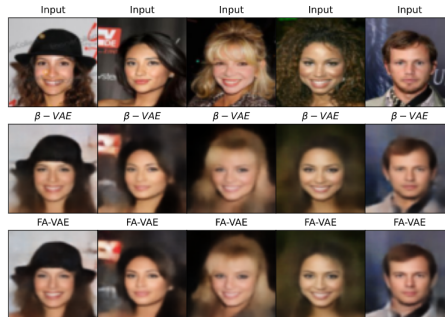


Figure 14: Images reconstructed by β -VAE and by FA-VAE

Model	Samples	R2 score
Multi-VAE	10000	0.855 ± 0.154
β -VAE	10000	0.941 ± 0.032
FA-VAE	10000	0.969 ± 0.027

Table 2: Reconstruction performance measured in R2 score over 10,000 CelebA test samples.



Figure 15: Latent space evolution. Each row represents the 10 most relevant features based on absolute value. The red column represents the image generated by the model without any modification. Then, all images at the left of the red column are images generated by arbitrarily decreasing the value of each feature. Likewise, all images at the right of the red column are images generated by increasing the value of each component.

interval.

For β -VAE, in Fig. 15a each row represents one of the 10 most relevant features. The \mathbf{z} latent space shows that there are 3 features with visual interpretation. Blue rows show that we can control facial hair by increasing or decreasing its value. Besides, the green row shows an impact on the image’s contrast. However, the remaining features do not present an explainable visual impact on the images.

Fig 15b shows the same analysis over FA-VAE, revealing that FA-VAE’s private latent space significantly outperforms β -VAE’s in both explainability and cleanliness terms. 9 out of the 10 most relevant features have a visual interpretation. For example, the golden marked latent features control the skin tone and the rotation of the face. The green rows contain the gender and the hairstyle, the blue row controls the background color between cold and warm, and, the gray marked latent features control the smiling. Moreover, we can see that the proposed model is capable of focusing on face information and filtering noisy backgrounds in the latent space.

4. Conclusions

This paper presents the FA-VAE model, the first deep hierarchical VAE for mixed and heterogeneous data using an interpretable FA latent space. FA-VAE is capable of conditioning multiple VAEs creating a model that can work with numerous data domains, from multi-label to continuous, binary, categorical, or even image data, depending on the VAE architecture. This conditioning is performed by a deep hierarchical structure using FA, learning a disentangled and explainable latent space.

Besides, given the multiview capability of this model, we have shown how we can perform domain adaptation between two different databases while conditioning them on external attributes outperforming state-of-the-art (SOTA) models. In addition, FA-VAE is the first model able to perform transfer learning between generative models, thus accelerating the learning process and even improving the performance. Hence, FA-VAE provides a robust model capable of dealing with real-world data sets.

Acknowledgements

This work was supported by MCIN AEI 10.13039 501100011033 [grant numbers RTI2018-099655-B-100, PID2020-115363RB-I00, PID2021-123182OB-I00, TED2021-131823B-I00]; the Comunidad de Madrid [grant numbers IND2018/TIC-9649, Y2018/TCS-4705]; the European Union (FEDER and the European Research Council (ERC) through the European Unions Horizon 2020 research innovation program [grant number 714161]; and the IISGM [grant INTRA-MURAL]. The authors would like to thank Emese Sükei for proofreading the manuscript.

References

- [1] S. Liu, L. Duan, Z. Zhang, X. Cao, Hierarchical multimodal fusion for ground-based cloud classification in weather station networks, *IEEE Access* 7 (2019) 85688–85695.
- [2] M. Bijelic, T. Gruber, F. Mannan, F. Kraus, W. Ritter, K. Dietmayer, F. Heide, Seeing through fog without seeing fog: Deep multimodal sensor fusion in unseen adverse weather, in: *Proceedings of the IEEE/CVF Conference on Computer Vision and Pattern Recognition*, 2020, pp. 11682–11692.
- [3] B. Rodríguez-Sánchez, A. Candela, M. J. Arroyo, M. Sánchez-Cueto, M. Marín, E. Cercenado, G. Méndez, P. Muñoz, L. Mancera, D. Rodríguez-Temporal, Rapid discrimination of *pseudomonas aeruginosa* st175 isolates involved in a nosocomial outbreak using maldi-tof mass spectrometry and ftir spectroscopy coupled with machine learning, *Authorea Preprints*.

- [4] A. Guerrero-López, A. Candela, C. Sevilla-Salcedo, M. Hernández-García, P. Martínez-Olmos, R. Canton, P. Muñoz, R. del Campo, V. Gómez-Verdejo, B. Rodríguez-Sánchez, Development and validation of a maldi-tof-based model to predict extended-spectrum beta-lactamase and/or carbapenemase-producing in *klebsiella pneumoniae* clinical isolates, *bioRxiv*.
- [5] A. U. Hirte, M. Platscher, T. Joyce, J. J. Heit, E. Tranvinh, C. Federau, Realistic generation of diffusion-weighted magnetic resonance brain images with deep generative models, *Magnetic Resonance Imaging* 81 (2021) 60–66.
- [6] Y. Li, S. Mavromatis, F. Zhang, Z. Du, J. Sequeira, Z. Wang, X. Zhao, R. Liu, Single-image super-resolution for remote sensing images using a deep generative adversarial network with local and global attention mechanisms, *IEEE Transactions on Geoscience and Remote Sensing* 60 (2021) 1–24.
- [7] H. Chen, X. He, H. Yang, J. Feng, Q. Teng, A two-stage deep generative adversarial quality enhancement network for real-world 3d ct images, *Expert Systems with Applications* 193 (2022) 116440.
- [8] T. Brown, B. Mann, N. Ryder, M. Subbiah, J. D. Kaplan, P. Dhariwal, A. Neelakantan, P. Shyam, G. Sastry, A. Askell, et al., Language models are few-shot learners, *Advances in neural information processing systems* 33 (2020) 1877–1901.
- [9] Z. Zheng, A. Ma, L. Zhang, Y. Zhong, Deep multisensor learning for missing-modality all-weather mapping, *ISPRS Journal of Photogrammetry and Remote Sensing* 174 (2021) 254–264.
- [10] J. H. Xu, K. Shinden, M. P. Kato, Table caption generation in scholarly documents leveraging pre-trained language models, in: *2021 IEEE 10th Global Conference on Consumer Electronics (GCCE)*, IEEE, 2021, pp. 963–966.
- [11] H.-H. Wu, P. Seetharaman, K. Kumar, J. P. Bello, Wav2clip: Learning robust audio representations from clip, in: *ICASSP 2022-2022 IEEE International Conference on Acoustics, Speech and Signal Processing (ICASSP)*, IEEE, 2022, pp. 4563–4567.
- [12] Z. Borsos, R. Marinier, D. Vincent, E. Kharitonov, O. Pietquin, M. Sharifi, O. Teboul, D. Grangier, M. Tagliasacchi, N. Zeghidour, Audioldm: a language modeling approach to audio generation, *arXiv preprint arXiv:2209.03143*.
- [13] J. Yi, R. Fu, J. Tao, S. Nie, H. Ma, C. Wang, T. Wang, Z. Tian, Y. Bai, C. Fan, et al., Add 2022: the first audio deep synthesis detection challenge, in: *ICASSP 2022-2022 IEEE International Conference on Acoustics, Speech and Signal Processing (ICASSP)*, IEEE, 2022, pp. 9216–9220.
- [14] C. K. Sønderby, T. Raiko, L. Maaløe, S. K. Sønderby, O. Winther, Ladder variational autoencoders, *Advances in neural information processing systems* 29.

- [15] A. Klushyn, N. Chen, R. Kurle, B. Cseke, P. van der Smagt, Learning hierarchical priors in vaes, *Advances in neural information processing systems* 32.
- [16] M. Vasco, H. Yin, F. S. Melo, A. Paiva, Leveraging hierarchy in multimodal generative models for effective cross-modality inference, *Neural Networks* 146 (2022) 238–255.
- [17] Y. Hong, M. Mundt, S. Park, Y. Uh, H. Byun, Return of the normal distribution: Flexible deep continual learning with variational auto-encoders, *Neural Networks* 154 (2022) 397–412.
- [18] M. J. Vowels, N. C. Camgoz, R. Bowden, Nestedvae: Isolating common factors via weak supervision, in: *Proceedings of the IEEE/CVF Conference on Computer Vision and Pattern Recognition*, 2020, pp. 9202–9212.
- [19] I. Peis, P. M. Olmos, A. Artés-Rodríguez, Unsupervised learning of global factors in deep generative models, *arXiv preprint arXiv:2012.08234*.
- [20] I. Peis, C. Ma, J. M. Hernández-Lobato, Missing data imputation and acquisition with deep hierarchical models and hamiltonian monte carlo, *arXiv preprint arXiv:2202.04599*.
- [21] H. Kojima, T. Ikegami, Organization of a latent space structure in vae/gan trained by navigation data, *Neural Networks* 152 (2022) 234–243.
- [22] A. L. Caterini, A. Doucet, D. Sejdinovic, Hamiltonian variational auto-encoder, *Advances in Neural Information Processing Systems* 31.
- [23] M. Suzuki, K. Nakayama, Y. Matsuo, Joint multimodal learning with deep generative models, *arXiv preprint arXiv:1611.01891*.
- [24] Y. Li, Y. Zhang, C. Yang, Unsupervised domain adaptation with joint adversarial variational autoencoder, *Knowledge-Based Systems* (2022) 109065.
- [25] M. Wu, N. Goodman, Multimodal generative models for scalable weakly-supervised learning, *Advances in Neural Information Processing Systems* 31.
- [26] M. Lee, V. Pavlovic, Private-shared disentangled multimodal vae for learning of latent representations, in: *Proceedings of the IEEE/CVF Conference on Computer Vision and Pattern Recognition*, 2021, pp. 1692–1700.
- [27] Y. Shi, B. Paige, P. Torr, et al., Variational mixture-of-experts autoencoders for multi-modal deep generative models, *Advances in Neural Information Processing Systems* 32.
- [28] W. Youpeng, L. Hongxiang, G. Yiju, Z. Liang, Amvae: Asymmetric multimodal variational autoencoder for multi-view representation, in: *International Conference on Artificial Neural Networks*, Springer, 2021, pp. 391–402.

- [29] J. Xu, Y. Ren, H. Tang, X. Pu, X. Zhu, M. Zeng, L. He, Multi-vae: Learning disentangled view-common and view-peculiar visual representations for multi-view clustering, in: Proceedings of the IEEE/CVF International Conference on Computer Vision (ICCV), 2021, pp. 9234–9243.
- [30] C. Sevilla-Salcedo, V. Gómez-Verdejo, P. Olmos, Sparse Semi-supervised Heterogeneous Interbattery Bayesian Analysis, Pattern Recognit. doi:10.1016/j.patcog.2021.108141.
- [31] D. P. Kingma, M. Welling, Auto-encoding variational bayes, arXiv preprint arXiv:1312.6114.
- [32] C. Sevilla-Salcedo, A. Guerrero-López, P. M. Olmos, V. Gómez-Verdejo, Bayesian sparse factor analysis with kernelized observations, Neurocomputing.
- [33] C. Bishop, Bayesian pca, in: M. Kearns, S. Solla, D. Cohn (Eds.), Advances in Neural Information Processing Systems, Vol. 11, MIT Press, 1998.
URL <https://proceedings.neurips.cc/paper/1998/file/c88d8d0a6097754525e02c2246d8d27f-Paper.pdf>
- [34] D. M. Blei, A. Kucukelbir, J. D. McAuliffe, Variational inference: A review for statisticians, Journal of the American statistical Association 112 (518) (2017) 859–877.
- [35] C. P. Burgess, I. Higgins, A. Pal, L. Matthey, N. Watters, G. Desjardins, A. Lerchner, Understanding disentangling in β -vae, arXiv preprint arXiv:1804.03599.
- [36] Z. Liu, P. Luo, X. Wang, X. Tang, Deep learning face attributes in the wild, in: Proceedings of International Conference on Computer Vision (ICCV), 2015.
- [37] I. Higgins, L. Matthey, A. Pal, C. Burgess, X. Glorot, M. Botvinick, S. Mohamed, A. Lerchner, beta-vae: Learning basic visual concepts with a constrained variational framework.
- [38] A. Royer, K. Bousmalis, S. Gouws, F. Bertsch, I. Mosseri, F. Cole, K. Murphy, Xgan: Unsupervised image-to-image translation for many-to-many mappings, in: Domain Adaptation for Visual Understanding, Springer, 2020, pp. 33–49.

Appendix A. Experiments

In this appendix, we add different experiments that demonstrate the potential of FA-VAE. The structure follows the same order as in the main article.

Appendix A.1. FA-VAE as a conditioned generative model

Following the experiment shown in Section 3.1, we demonstrate that we can also generate random conditioned faces.

To analyze it, we show how the proposed model can generate images conditioned to specific attributes. We proceed as follows: (i) we create random $\mathbf{x}_{n,:}^{(A)}$ multilabel vectors using [wearing lipstick, gender, smiling] binary notation, (ii) we create their real pseudo-observation $\mathbf{z}_{n,:}^{(A)}$, (iii) we generate the posterior distribution of $\mathbf{g}_{n,:}$ given $\mathbf{z}_{n,:}^{(A)}$ which follows a Gaussian distribution with parameters:

$$\begin{aligned}\Sigma_{\mathbf{g}_{n,:}}^{-1} &= I_{K_c} + \tau^{(A)} \mathbf{W}^{(A)T} \mathbf{W}^{(A)} \\ \mu_{\mathbf{g}_{n,:}}^* &= \tau^{(A)} \mathbf{z}_{n,:}^{(A)} \mathbf{W}^{(A)} \Sigma_{\mathbf{g}_{n,:}}^*,\end{aligned}\tag{A.1}$$

(iv) we sample $\mathbf{z}_{n,:}^{(O)} \sim \mathcal{N}(\mathbf{g}_{n,:}^*, \mathbf{W}^{(O)}, \tau^{(O)})$, and, finally (v) we use FA-VAE’s generative distribution $p_{\theta}(\mathbf{o}_{n,:} | \mathbf{z}_{n,:}^{(O)})$ to sample artificially generated conditioned images. Fig. A.16 shows these images generated by 8 random $\mathbf{x}_{n,:}^{(A)}$ multilabel attributes.

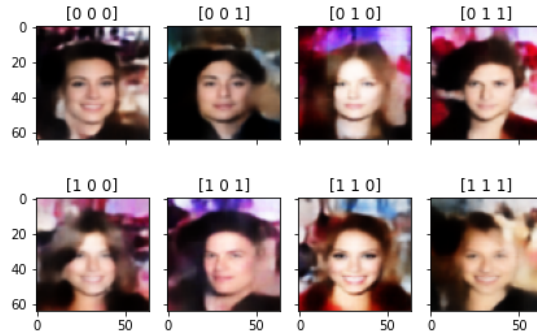


Figure A.16: Fake faces generated by random $\mathbf{x}_{n,:}^{(A)}$ vectors. The title of each image indicates which attribute is activated: smiling, wearing lipstick, and gender. For example, [1 0 0] means a smile [1] without lipstick [0] in a woman’s face [0], and [1 0 1] means a smile [1] without lipstick [0] in a male’s face [1].

We can quickly condition a pre-trained VAE to arbitrary attributes by training 150 epochs of FA-VAE.

Appendix A.2. Domain adaptation

Following the experiment described in Section 3.2, we show that the global latent variable is also complete and continuous.

Similarly, as did in 3.2 with the private latent space interpolation, we could implement such interpolation directly from the global space by sampling from $\mathbf{g}_{n,:}$ and generating a sample that both domains can understand. The next two examples illustrate that behavior. Again, we select two new CelebA observations, and we project them to the global space \mathbf{G} as $\mathbf{g}_{1,:}$ and $\mathbf{g}_{2,:}$. Then, we calculate $\mathbf{g}_{\lambda,:}$ following Eq. (13). For this scenario, each generative network decodes $\mathbf{g}_{\lambda,:}$ creating a pair of images. In Fig. A.17 the reconstructed sequences $\mathbf{x}_{\lambda,:}^{(m)} | \mathbf{g}_{\lambda,:}$ are shown.



Figure A.17: Example of an image transformation and domain adaptation application using a common global representation $\mathbf{g}_{\lambda,:}$. The first row shows images generated by the CelebA VAE while the second row shows images generated by the Cartoon VAE.

Each one of the $\mathbf{g}_{\lambda,:}$ generates meaningful content showing completeness. However, there is a trade-off between both domains. On the one hand, the CelebA domain shows better continuity leading to a clear transition between both images. On the other hand, the Cartoon domain, characterized by a discrete set of features, shows better completeness where every $\mathbf{g}_{\lambda,:}$ creates a cartoon avatar without any distortion or artifact.